



Università degli Studi di Pavia

FACOLTÀ DI SCIENZE MATEMATICHE, FISICHE, NATURALI
Corso di laurea in Scienze Fisiche

Fotorivelatori Criogenici per la rivelazione di eventi rari in fisica delle alte energie

Candidato

Alessandro Villa

Matricola 462495

Supervisore

Dott. Andrea Negri

Co-Supervisor

Dott. Roberto Ferrari

Dott. Lorenzo Pezzotti

Indice

Introduction	iii
1 Future $e^+ e^-$ colliders	1
1.1 Physics goals	1
1.2 Leptonic colliders	1
1.3 Detectors	1
2 Calorimetry and dual-readout	3
2.1 Electromagnetic showers	3
2.1.1 Shower development	3
2.1.2 Energy resolution	3
2.2 Hadronic showers	3
2.2.1 Shower development	3
2.2.2 Energy resolution	3
2.3 Dual-readout calorimetry	3
2.3.1 Working principles	4
2.3.2 Experiments	4
3 Silicon Photomultipliers	5
3.1 Working principles	5
3.2 SiPM Response	5
3.3 Noise effects	5
3.3.1 Dark Count Rate	5
3.3.2 After-Pulse	5
3.3.3 Optical Cross-Talk	5
4 IDEA DR calorimeter project	7
5 IDEA DR calorimeter full simulation	9
5.1 Simulation structure	10
5.1.1 Calorimeter simulation	10
5.1.2 SiPM response digitization	12
5.2 Simulation performances	14
5.2.1 Different configurations	14

5.2.2	Time studies	14
5.2.3	Occupancy effect	18
5.2.4	Energy resolution	18
5.3	Neural Network: Particle ID on waveform	18
5.3.1	Configuration	18
5.3.2	Performances	18
5.4	Neural Network: Particle ID on imaging	18
5.4.1	Configuration	18
5.4.2	Performances	18
6	Conclusion	19
	Thanks	21
	Bibliography	23

Introduction

aaa

Capitolo 1

Future $e^+ e^-$ colliders

aaa

1.1 Physics goals

aaa

1.2 Leptonic colliders

aaa

1.3 Detectors

Capitolo 2

Calorimetry and dual-readout

aaa

2.1 Electromagnetic showers

aaa

2.1.1 Shower development

aaa

2.1.2 Energy resolution

aaa

2.2 Hadronic showers

aaa

2.2.1 Shower development

aaa

2.2.2 Energy resolution

aaa

2.3 Dual-readout calorimetry

aaa

2.3.1 Working principles

aaa

2.3.2 Experiments

Capitolo 3

Silicon Photomultipliers

aaa

3.1 Working principles

aaa

3.2 SiPM Response

aaa

3.3 Noise effects

aaa

3.3.1 Dark Count Rate

aaa

3.3.2 After-Pulse

aaa

3.3.3 Optical Cross-Talk

Capitolo 4

IDEA DR calorimeter project

aaa

Capitolo 5

IDEA DR calorimeter full simulation

As already said, the project described in chapter 4 is an on-going production and has to be supported by simulation. With this goal, a dual-readout calorimeter full simulation has been developed allowing to generate data and monitor the whole process from the collision on the interaction point to the digitized signal produced by SiPMs.

The chapter presents a description of the simulation structure. The section 5.1 describes in details the simulation dividing it in two main Monte Carlo processes:

- the calorimeter simulation, coded in GEANT4;
- the SiPM response digitization ("pySIPM"), coded in Python.

Later, the performances obtained will be shown. The temporal behavior, the SiPM saturation effect and the energy resolution will be described in section 5.2.

The second half of the chapter treats of the possibility of simple particle identification using neural network structures.

In section 5.3 neural networks working on digitized waveforms are described. The aim of these neural network is to correctly distinguish waveforms generated by electrons (e^-) or pions (π^-) in a range of energy from 20 to 80 GeV.

The last section (sec.5.4) exposes another type of neural networks. These have the purpose of identify if signal are generated from photons (γ) or neutral pions (π^0) analyzing the spazial pattern of energy released in the calorimeter.

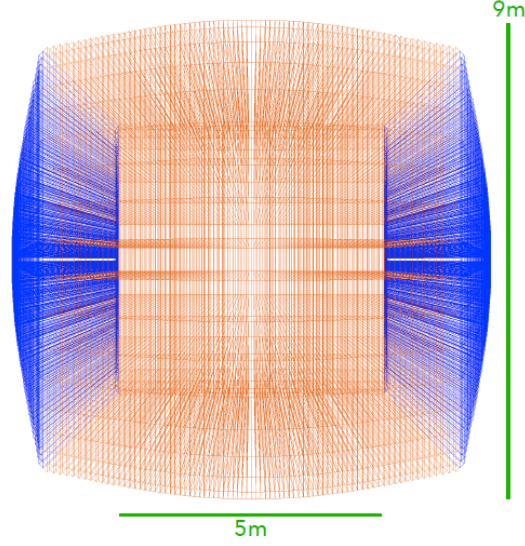


Figura 5.1: Calorimeter geometry.

5.1 Simulation structure

5.1.1 Calorimeter simulation

Following the idea show in chapter 4, the calorimeter simulated is sketched in figure 5.1. As can be seen, it has a cylindrical symmetry characterized by a barrel and two endcaps. This 4π structure is obtained rotating 36 simpler component, called slices, around the z axis. The dimensions of the slices are shown in figure 5.2, therefore the inner diameter and the inner length are both 5 m meanwhile the overall outer diameter and length are 9 m.

Each half slice is composed by 75 2 m long towers (40 part of the barrel and 35 part of the endcap), 5400 of this element are used to set up the whole calorimeter. To correctly cover an almost 4π solid angle each tower has different trapezoidal inner face with dimensions that can vary from ~ 5 cm to ~ 8 cm. A small circular area, with 0.25 m of radius, centered along the z axis is not covered by the calorimeter to permit the beam to reach the interaction point (IP).

The towers are copper based and play the role of absorber. To have a sensitive element they are filled by optical fibres. The idea of a projective calorimeter make the absorber volume greater increasing the distances from the IP. New fibres at different depth have to be placed inside the calorimeter to keep constant the sampling fraction.

As the dual-readout technique needs to distinguish Scintillating (S) and Cherenkov (C) signal, two types of fibres are used (fig. 5.3). Their charac-

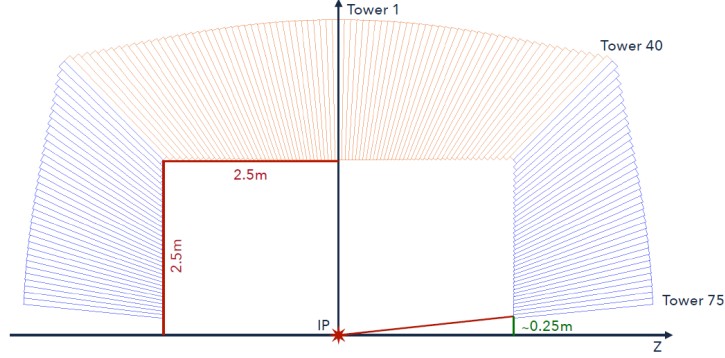


Figura 5.2: Calorimeter single slice.

Kuraray SCSF-78 (<i>S</i>)	
Core:	$r = 0.485 \text{ mm}$, Polystyrene (C_5H_5), $\rho = 1.95 \text{ g/cm}^3$, $n = 1.59$
Cladding:	Thickness = 2% of r , PMMA ($C_5H_8O_2$), $\rho = 1.19 \text{ g/cm}^3$, $n = 1.49$
Main properties:	Emission constant = 2.8 ns , LY = 10^4 photons/MeV , $\lambda_{att} = 4 \text{ m}$
Mitsubishi SK-40 (<i>C</i>)	
Core:	$r = 0.485 \text{ mm}$, PMMA ($C_5H_8O_2$), $\rho = 1.19 \text{ g/cm}^3$, $n = 1.49$
Cladding:	Thickness = 2% of r , Fluorinated Polymer (C_2F_2), $\rho = 1.43 \text{ g/cm}^3$, $n = 1.42$
Main properties:	$\lambda_{att} = 8.9 \text{ m}$

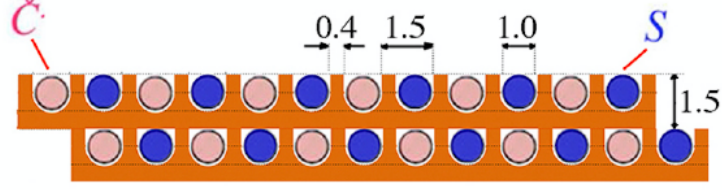
Tabella 5.1: fibres *S* and *C*.

teristic are shown in tab. 5.1.

The fibre refractive indices determine the light transport (as consequence of the Snell's law [2]). The signal from the scintillating fibres is parametrised by the deposited energy while the Cherenkov photons are produced accordingly to the Cherenkov emission process.

For each event, the simulation gives as output useful information:

- Event ID;
- Fibre Type;
- Fibre ID;
- the position of the fibre end closer to the IP;

Figura 5.3: Fibres C and S .

- the number of photons reaching the fibre further end;
- the list of photons time of arrival to the fibre end.

The computation of light propagation is extremely time consuming, so that it has to be fine tuned to optimize the process. In particular, the propagation of C photons is tracked until the single photon reach the core-cladding boundary (i.e. at the distance R from the further end of the fibre and at the time t_0). If the emission angle is inside the range of the fibre numerical aperture, the photon is added to the final number of photons (after a Poissonian smearing on their number). The time of arrival on the sensor for each photon is estimated as:

$$t_C = t_0 + R \frac{n_C}{c} \quad (5.1)$$

where $n_C = 1.49$ is the fibre refractive index and c is the speed of light.

The S fibres, instead, carry scintillating photons produced considering the light yield of the fibres and the energy deposited by the interacting particle. The number of photons is smeared with as Poissonian law and de time of arrival on the sensor is obtained as:

$$t_S = t_0 + R \frac{n_S}{c \times \cos(\vartheta)} + t^* \quad (5.2)$$

where $n_S = 1.59$ is the refractive index and t^* is a random time that considers the fibres decay time, it is chosen from an exponential distribution with 2.8 ns as mean value. Considering the internal reflection, the photon path depends on the ϑ angle (i.e. the angle between the photon direction and the fibre axis). It is chosen randomly in the range $[\cos(\alpha), \cos(0)]$, where $\alpha = 20.4^\circ$ is the fibre critical angle.

5.1.2 SiPM response digitization

The results obtained are the input of the second part of the simulation: *pySiPM*, a Monte Carlo simulation, performed mostly in Python, able to

reproduce the SiPM response to a light source and replicate the waveforms recorded with a digitizer [3].

The importance of this software goes beyond our context, but perfectly fits our needs. In particular each fibre from the calorimeter simulation is considered coupled to a single SiPM, which digitized response is simulated through *pySiPM*.

The simulation allows to set most of the SiPM parameters:

- **Geometrical parameters:** the sensor dimensions and the pixel pitch.
- **Sensor parameters:** Photon Detection Efficiency, Dark Count Rate, After-Pulse probability, Optical Cross-Talk probability.
- **Signal parameters:** rise time constant, decay time constant.
- **Waveform parameters:** time window, sampling time, integration window.

For each event and fibre, random parameters determine the photon position inside the sensor. Meanwhile the sensor PDE is tuned to have consistent mean values of $\sim 400 \text{ Spe/GeV}$ and $\sim 100 \text{ Cpe/GeV}$ respectively for S and C light yield. A control stop the count of impinging photons on the same cell to a maximum one, then each element of noise is generated with the set probability.

The pulse generated is a combination of two exponentials characterized by the rise time constant (τ_{rise}) and the decay time constant (τ_{fall}), considering the different photon time of arrival (t_S and t_C):

$$y(t) = A \cdot \left(e^{-\frac{t}{\tau_{fall}}} - e^{-\frac{t}{\tau_{rise}}} \right). \quad (5.3)$$

The total signal of each SiPM is the sum of all the signals generated from the activated cells.

The information given as output of the simulation are:

- **Data reported from GEANT4 simulation:** event ID, type of fibre, fibre ID, fibre position;
- **Computed quantities:** integral, peak height, time of arrival, time over threshold, time of peak;
- **Digitized waveform.**

Geometrical Parameter	
SiPM area	$1 \times 1 \text{ mm}^2$
Sensor Parameters	
DCR	200 kHz
After-Pulse	3%
Cross-Talk	1%
Signal Parameter	
Rise time	1 ns
Waveform Parameters	
Time window	500 ns
Integration window	300 ns
Sampling frequency	10 GHz

Tabella 5.2: parameter

5.2 Simulation performances

5.2.1 Different configurations

The results shown in this last chapter are obtained considering different SiPM parameters configurations.

They have been chosen in a common parameter space identified checking the lineup of SiPMs produced by Hamamatsy [4]. Two are the parameters that has been changed in our studies:

- the decay time constant of the signal, the chosen values are 10 ns and 50 ns ;
- the pixel size, the chosen values are $10 \text{ }\mu\text{m}$, $15 \text{ }\mu\text{m}$ and $25 \text{ }\mu\text{m}$.

The other fixed values of parameters are listed in the table 5.2.

An example of waveform generated is plotted in figure 5.4 where is clear the difference produced using two different decay time constant.

5.2.2 Time studies

An important aspect that has to be studied is the temporal one. In order to do this, data of 1000 events are produced. In each event a 40 GeV electron is produced from the interaction point.

A first step is to analyze the distribution of the time of arrival of the photons converted at the SiPMs (i.e. the time recorded in the GEANT4 simulation output).

The distribution obtained from C and S photons are plotted in figure 5.5.

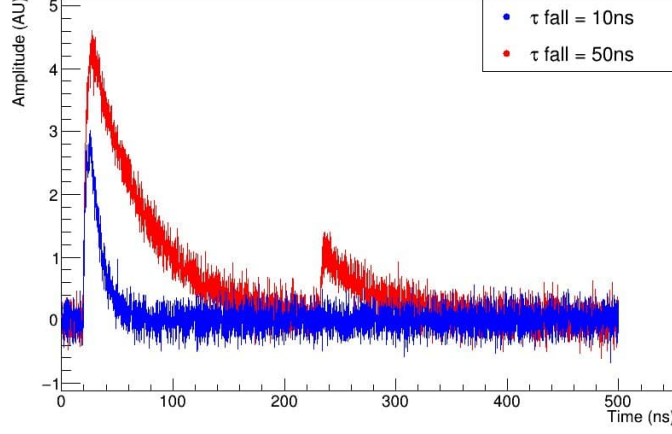


Figure 5.4: Single waveform

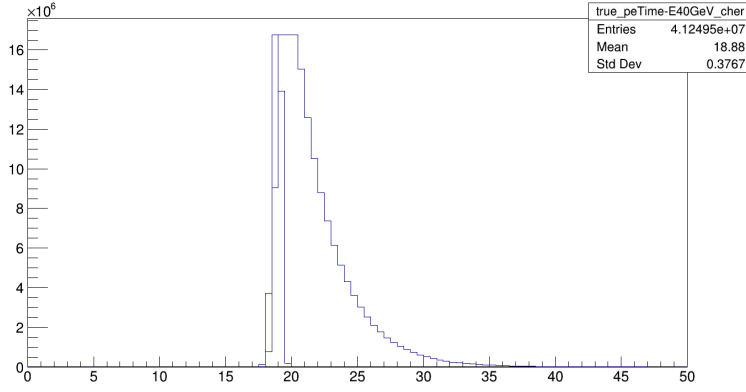


Figure 5.5: True time of arrival distribution.

As expected, the distribution of C photons time extremely narrow due to the instantaneous production of photons at the passage of relativistic charged particle in the fibres, instead the S photons time distribution shows an exponential tail that is a direct consequence of the emission time constant of the Polystyrene.

Now a step forward can be done using this data as input for *pySiPM*. The SiPM parameters are chosen as described in paragraph 5.2.1. In this context the most interesting editable parameter is the decay time constant. Figure ?? and ?? are in analogy with respect to the last described and presents clearly a widening of the distributions, the cause of this phenomenon has to be associated to the characteristic response function of the sensors 5.3.

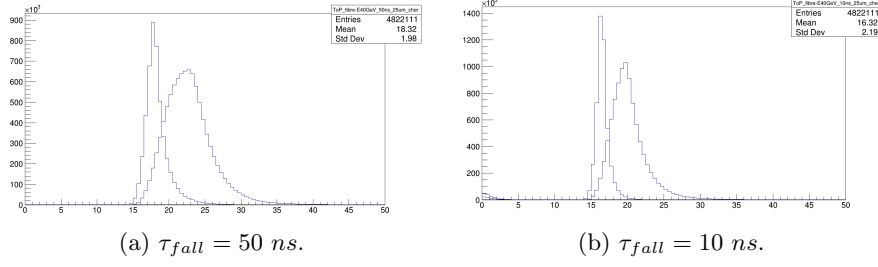


Figura 5.6: time of peak distribution.

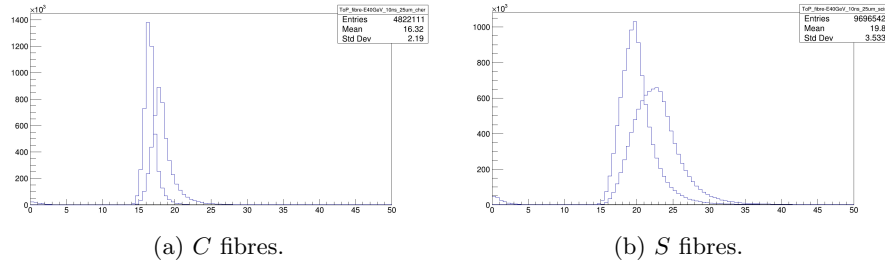


Figura 5.7: time of peak distribution.

These data can be compared looking for differences in changing SiPMs configurations. As we can see in figure 5.7, the same C and S photons produce narrower time of peak distribution due to the less impact of electronic noise on a sharper response function.

The impact of noise on time of peak precision is also dependent on the number of photons impinging the same SiPM, in particular the peak precision increase with the number of photons.

To prove this 10000 SiPMs have been fired with each time increasing number of simultaneous photons. For each fixed number of photons, the time of peak has been recorded, plotted in an histogram and fitted with a Gaussian function. An example of these histograms is shown in figure 5.8.

The standard deviation of these Gaussian fit is the interested quantity that has been recorded and reported in the table 5.3.

It is interesting to plot these data and study the behavior of the standard deviation in function of the number of photons. Figure 5.9 shows graphically the data, which are well fitted with a function of the form:

$$\sigma = \frac{A}{\sqrt{n}} + B. \quad (5.4)$$

The parameters obtained are $A = 0.8712 \text{ ns}$ and $B = 0.08734 \text{ ns}$ for data associated to SiPMs with $\tau_{fall} = 10 \text{ ns}$, and $A = 1.949 \text{ ns}$ and $B = 0.008217 \text{ ns}$ for data associated to SiPMs with $\tau_{fall} = 50 \text{ ns}$.

Number of photons	σ with $\tau_{fall} = 10 \text{ ns}$ [ns]	σ with $\tau_{fall} = 50 \text{ ns}$ [ns]
1	1.4150	7.0680
2	0.8717	2.6420
3	0.6738	1.7370
4	0.5742	1.3770
5	0.5146	1.1230
6	0.4624	0.9719
7	0.4314	0.9148
8	0.3998	0.8508
9	0.3811	0.7717
10	0.3605	0.7169
25	0.2339	0.4481
50	0.1679	0.3112
100	0.1229	0.2297

Tabella 5.3: Sigmas

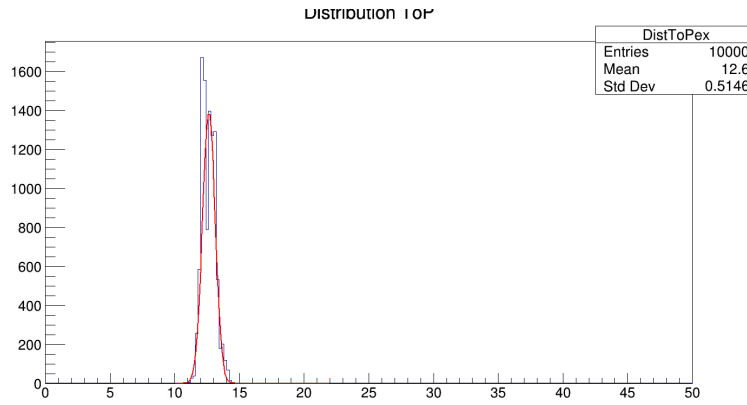


Figura 5.8: Time of peak dummy, 5 photons, 50 ns.

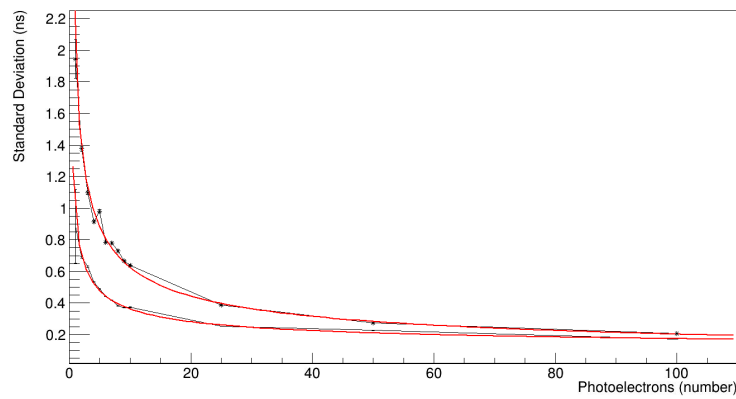


Figura 5.9: Time of peak dummy, 5 photons, 50 ns.

5.2.3 Occupancy effect

aaa

Occupancy effect and Energy loss

Studies of the occupancy effect are important preliminary studies that give knowledge about the information loss in the detection process.

5.2.4 Energy resolution

aaa

5.3 Neural Network: Particle ID on waveform

aaa

5.3.1 Configuration

aaa

5.3.2 Performances

aaa

5.4 Neural Network: Particle ID on imaging

aaa

5.4.1 Configuration

aaa

5.4.2 Performances

aaa

Capitolo 6

Conclusion

aaa

Thanks

aaa

Bibliografia

- [1] Y. Fukuda et al., Phys. Rev. Lett. 81 (1998) 1158-1162.
- [2] Y. Fukuda et al., Phys. Rev. Lett. 81 (1998) 1158-1162.
- [3] Y. Fukuda et al., Phys. Rev. Lett. 81 (1998) 1158-1162.
- [4] Hamamatsu SiPMs lineup https://www.hamamatsu.com/eu/en/product/optical-sensors/mppc/mppc_mppc-array/all_products/index.html